Simulation of Primary Breakup for Diesel Spray with Phase Transition

Peng Zeng [1], Bernd Binninger and Norbert Peters
Institute for Combustion Technology
RWTH Aachen, Templergraben 64, 52056 Aachen, Germany
Marcus Herrmann
Department of Mechanical and Aerospace Engineering
Arizona State University , Tempe, AZ 85287-6106, USA

Abstract

A continuum formalism for describing the behavior of primary atomization with phase transition is presented, which includes the effects of heat and mass transfer of the two phase flow, the formation of ligaments and droplets, surface tension force and turbulence. Simulation of liquid jet primary atomization given by Marcus Herrmann (A balanced force refined level–set grid method for two–phase flows on unstructured flow solver grids, Journal of Computational Physics 2008) is extended to include the effects of evaporation and its relative motion of the interface between gaseous and liquid phase. It is shown that the phase transition process can be modeled by introducing a laminar surface regression velocity, which is derived from the temperature boundary layer. It is shown that the phase transition effect has a big impact on the the spray primary breakup processes.

Introduction

Numerical simulation of diesel engine combustion has become an important tool in engine development. One major issue in the modeling of turbulent reactive flows is the turbulent spray that accompanies fuel injection. One way to model the injection process is to use the level–set method to describe the physical details of spray breakup; especially, primary breakup, the very first fragmentation process when liquid column rushes out of a nozzle, forming ligaments and breaking up into primary droplets [2].

If liquid fuel is injected into the combustion chamber, the high ambient temperature will enhance the phase transition process from liquid fuel to fuel vapor. Fig. 1 shows slow and fast evaporation processes, leading to totally different sprays: the upper injection by $T = 293$K, the lower case by $T = 800$K. In order to simulate diesel injection(characterized by strong evaporation), the level–set method has to include the phase transition effect.

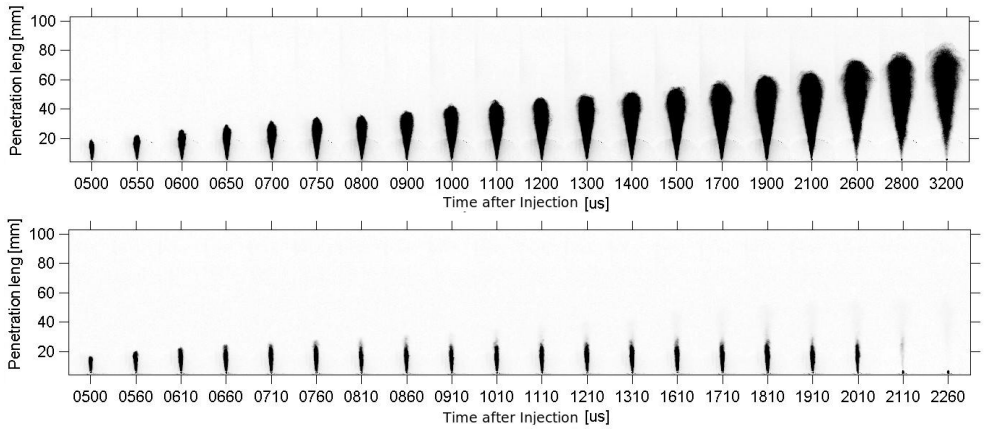

Figure 1: Spray liquid–phase penetration with different ambient temperatures

In the following sections, firstly, the original level-set method is briefly described. Then, the phase transition model will be introduced. After that, direct numerical simulation for diesel spray and its result will be discussed.

[1]Corresponding author: p.zeng@itv.rwth-aachen.de

Two-Phase flow using Level-Set method

The two-phase flow is described in one-fluid formulation, liquid and vapor phases have their own fluid properties, i.e., density, viscosity, surface tension, etc. The flow is governed by the unsteady Navier-Stokes equations in the variable density incompressible limit [1, 2],

$$\nabla \cdot \boldsymbol{u} = 0 \tag{1}$$

$$\frac{\partial \boldsymbol{u}}{\partial t} + \boldsymbol{u} \cdot \nabla \boldsymbol{u} = -\frac{1}{\rho}\nabla p + \frac{1}{\rho}\nabla \cdot (\mu(\nabla \boldsymbol{u} + \nabla^T \boldsymbol{u})) + \boldsymbol{g} + \frac{1}{\rho}\boldsymbol{T}_\sigma \tag{2}$$

Surface tension force $\boldsymbol{T}_\sigma$ is non-zero only at the location of the phase interface $\boldsymbol{x}_f$

$$\boldsymbol{T}_\sigma(\boldsymbol{x}) = \sigma\kappa\delta(\boldsymbol{x} - \boldsymbol{x}_f)\boldsymbol{n} \tag{3}$$

The interface location $\boldsymbol{x}_f$ is described by a level–set scalar $G(\boldsymbol{x}_f, t) = 0$. In the gas, $G(\boldsymbol{x}_f, t) < 0$; in the liquid, $G(\boldsymbol{x}_f, t) > 0$. The level–set transport equation is

$$\frac{\partial G}{\partial t} + \boldsymbol{u} \cdot \nabla G = 0 \tag{4}$$

The interface normal vector can be expressed as

$$\boldsymbol{n} = \frac{\nabla G}{|\nabla G|} \quad , \tag{5}$$

and the interface surface curvature as

$$\kappa = \nabla \cdot \boldsymbol{n} \quad . \tag{6}$$

Phase Transition

As Fig. 2 shows, we consider an evaporating liquid with surface tension, which has a uniform temperature. The gaseous phase has much a higher temperature, leading to strong evaporation at the interface. Previous studies on spray primary breakup have not considered the phase transition effect on the interface behavior. The new element in this study is the introduction of surface regression velocity s_{SR} shown in Fig. 3, leading to a new interface evolution equation.

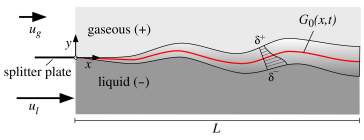

Figure 2: Problem Formulation

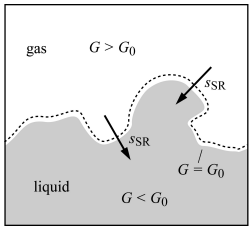

Figure 3: Surface Regression Velocity

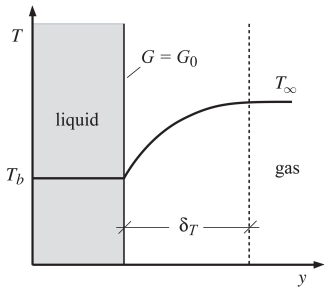

Figure 4: Temperature Boundary Layer

Starting from the balance of energy, we assume all the conducted heat at the interface $(\boldsymbol{x} = \boldsymbol{x}_f)$ is consumed by evaporation,

$$\frac{\rho_g \nu_g}{\mathrm{Pr}} \frac{\partial T}{\partial y}\bigg|_{\boldsymbol{x}=\boldsymbol{x}_f} = \frac{\dot{m} h_L}{C_p} \quad , \tag{7}$$

where $\dot{m} = \rho_l s_{\mathrm{SR}}$ is the mass flow rate per unit area, h_L is the latent heat of phase transition, C_p is the heat capacity of liquid phase, and Pr is the Prandtl number. Fig. 4 shows the temperature boundary layer, where δ_T is the boundary layer thickness which includes the length scale, T_b is the boiling temperature of the liquid phase, and T_∞ is the ambient temperature. In laminar cases, the surface regression velocity can therefore be modeled as

$$s_{\mathrm{SR}} = \frac{1}{\mathrm{Pr}} \frac{\rho_g}{\rho_l} \frac{C_p(T_\infty - T_b)}{h_L} \frac{\nu_g}{\delta_T} \quad . \tag{8}$$

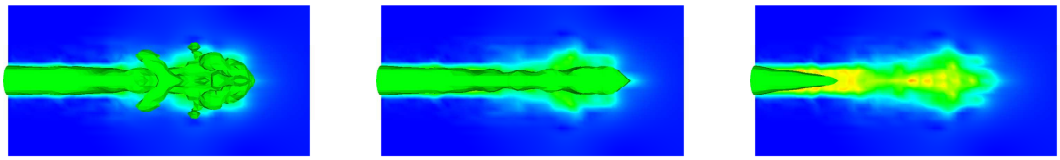

Figure 5: From left to right, $s_{SR} = 0.0, s_{SR} = 0.01, s_{SR} = 0.1$

The interface evolution equation can be found as

$$\frac{\partial G}{\partial t} + \boldsymbol{u} \cdot \nabla G + s_{SR} |\nabla G| = 0 \quad . \tag{9}$$

Fig. 5 shows different surface regression velocities will consequently generate different liquid-vapor phase interface for a laminar jet. Our asymptotic analysis of the boundary layers shows, the surface regression velocity has the formula

$$s_{SR} = \varepsilon s_{SR0} + \varepsilon^2 s_{SR1}, \quad \varepsilon^2 = 1/\mathrm{Re} \quad , \tag{10}$$

where the leading order term, s_{SR0}, is a function of temperature boundary layer thickness (8), and the first order term, s_{SR1}, contains the interface curvature. In order to include the local turbulent enhancement for heat and mass transfer, a turbulent surface regression velocity should be modeled statistically. Here we present a DNS with a presumed constant surface regression velocity.

Numerical methods

The interface evolution equation (9) is solved by using Refined Level-Set Grid (RLSG) method on an auxiliary, high-resolution equidistant Cartesian grid [4], while the Navier-Stokes equations (1) (2) are solved on their own computational grid. The remaining variables are expressed in terms of function based on the instantaneous position of the liquid-vapor interface. The main benefits of RLSG are: first, the local grid refinement can minimize the numerical error due to the truncation errors, leading to more accurate interface tracking; second, using an equidistant Cartesian grid allows high order numerical schemes to be easily applied with their full order of accuracy. More numerical detail about RLSG can be found in [4]. The RLSG solver LIT (Level set Interface Tracker) uses 5th order WENO scheme for space and 3rd order Runge-Kutta scheme for time discretization. The Navier-Stokes equations are spatially discretized using low-dissipation, finite-volume operators [3]. The flow solver CDP uses fully unstructured computational grid. A low-dissipation, finite-volume operators [3] spatially discretized the Navier-Stokes equations. CDP uses a second order Crank-Nicolson scheme for implicit time integration, and the fractional step method will remove the implicit pressure dependence in the momentum equations. Communication between the level–set solver and the flow solver is handled by the coupling software CHIMPS [6].

Computation Domain and Injection Conditions

The injection flow is characterized by a length scale of the injector nozzle diameter D, and a velocity scale of the central pipe inflow velocity U_0. The combustion chamber is simplified as a cylinder with radius R and length L. The coordinate system is located at the central point of the injector exit. Fig. 6 shows the computational domain. Table 1 gives the geometry setup for the simulation, as well as the injection condition used by Spiekermann et al.[7]. For the liquid phase, based on the Nozzle Diameter, D, and flow rate in the central pipe inflow, U_0, the Reynolds number is $\mathrm{Re}_l = \frac{\rho_l U_0 D}{\mu_l} \simeq 15 \times 10^4$, and the Weber number is $\mathrm{We}_l = \frac{\rho_l U_0^2 D}{\sigma} \simeq 27 \times 10^4$. The gas velocity at beginning is zero.

Boundary Conditions

For the flow solver, the inflow boundary condition is extracted from a precomputed turbulent single–phase pipe–flow with the same Reynolds number. The computational grids used in the periodic pipe-flow section are identical to those in the inlet section of the injection simulation. Tests were performed, verifying that the results of this inflow

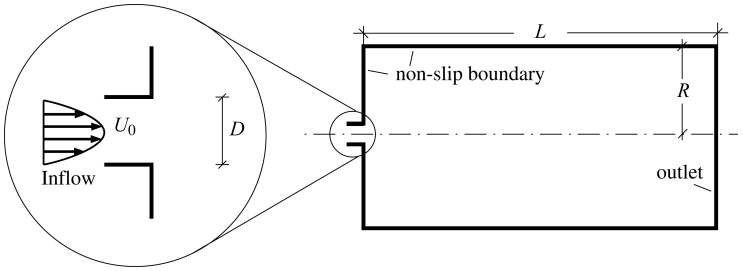

Figure 6: Computational domain

Nozzle Diameter D	0.138 mm
Chamber Length L	90 mm
Chamber Radius R	40 mm
Inflow Velocity Uo	300 m/s
Liquid Temperature T_l	550K
Liquid Density ρ_l	600 kg/m^3
Liquid Viscosity μ_l	$1.0 \times 10^{-4} Pa*s$
Liquid Surface Tension σ	0.025 N/m
Gas Temperature T_g	700K
Gas Density ρ_g	25 kg/m^3
Gas Viscosity μ_g	$1.0 \times 10^{-5} Pa*s$

Table 1: Computation Domain and Injection Conditions

boundary condition are in compliance with the statistical properties of a pipe flow. Two other boundary conditions are also used: a convective outflow boundary condition downstream at the exit, and a non–slip boundary condition for the rest (see Fig. 6). For the level–set solver, Dirichlet condition is used at the inflow nozzle and Neumann conditions are used for all the rest boundaries.

Computational Grid

The simulations use $256 \times 256 \times 512$ grid points in radial, azimuthal and axial directions for the flow solver, and the mesh is stretched in order to cluster grid points near the spray center, spacing the finest grid $\Delta x \simeq 3\eta \sim 4\eta$, where $\eta \simeq 1\mu$m is the Kolmogorov length coherent to the Reynolds number given before. The refined level–set grid has a half billion active cells. This combination was shown to yield promising results for primary breakup [5] [6].

Results

Fig. 9 shows snapshots of the turbulent liquid jet and droplets generated by primary breakup. The Lagrangian spray model, which removes the droplets from the ligaments and transfers into Lagrangian particles, can be found in [5]. Most of the droplets come from the mushroom tip at the jet head, complex topology and elongated ligaments have been observed. Compared with the atomization process without evaporation, the breakup of ligaments and droplet generation are much faster and more intensive. This can be explained in Fig. 7, which shows the curvature spectrum made from Fourier transformation of local curvature values along the ligaments with- and without evaporation. In the evaporation case, the large wavenumber of curvature fluctuations will promote the breakup processes.

Fig. 8 shows the droplet size distribution, ranging from the cut-off length scale that accompanies with the numerical grid size to large liquid blocks. Different from the atomization process without evaporation, more small droplets can be observed. With the help of equation (8), more realistic simulations will be presented in the future.

Summary and Outlook

An extension of the level–set method for primary breakup with phase transition has been presented. The surface regression velocity is introduced and the interface evolution equation has been derived. This model has been applied for a direct numerical simulation of a turbulent diesel injection, the spatial distribution and the distribution of the

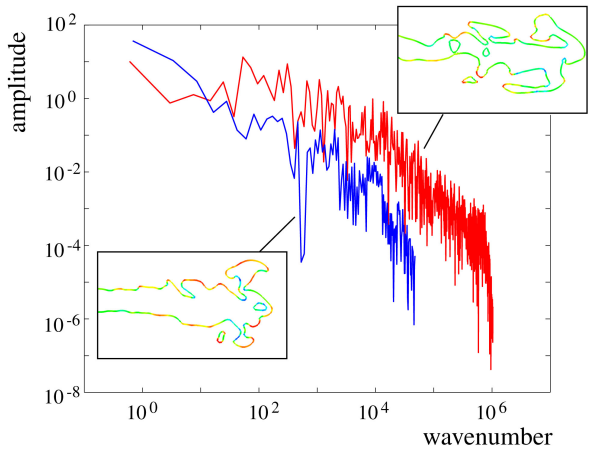

Figure 7: Curvature Spectrum,
with evaporation(red), without(blue)

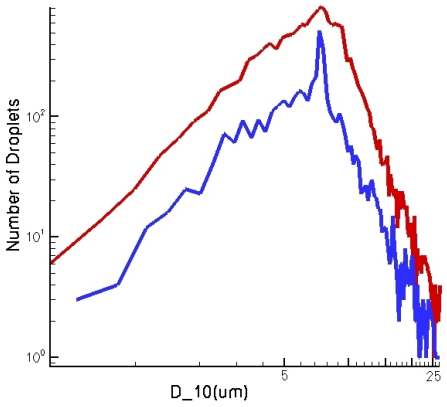

Figure 8: Droplet size distribution,
with evaporation(red), without(blue)

diameters of the droplets are simulated in this example. The mathematical model and the DNS solution presented here will provide the frame for a statistical simulation of the primary breakup within future large eddy simulations.

Acknowledgments

This work is financed by the German Research Foundation in the framework of DFG-CNRS research unit 563: Micro-Macro Modelling and Simulation of Liquid-Vapour Flows, (DFG reference No. Pe241/35-1).

Nomenclature

$\boldsymbol{g}$	gravitational acceleration	$\boldsymbol{u}$	flow velocity	Subscripts	
G	level–set scalar	$\boldsymbol{x}_f$	phase interface position		
h_L	latent heat			g	gas
$\boldsymbol{n}$	interface normal vector	ρ	density	l	liquid
p	pressure	μ	dynamic viscosity		
s_{SR}	surface regression velocity	κ	local mean surface curvature		
T	temperature	σ	surface tension coefficient		
$\boldsymbol{T}_\sigma$	surface tension force	δ_T	temperature boundary layer thickness		

References

[1] Carsten Baumgarten. *Mixture Formation in Internal Combustion Engines*. Springer, 2006.

[2] Mikhael Gorokhovski and Marcus Herrmann. Modeling primary atomization. *Annual Review of Fluid Mechanics*, 40:343–366, 2008.

[3] F. Ham, K. Mattsson, and G. Iaccarino. Accurate and stable finite volume operators for unstructured flow solvers. *Center for Turbulence Research Annual Research Briefs*, 2006.

[4] M. Herrmann. A balanced force refined level set grid method for two- phase flows on unstructured flow solver grids. *J. Comput. Phys.*, 227:2674–2706, 2008.

[5] M. Herrmann. Detailed numerical simulations of the primary breakup of turbulent liquid jets. *Proceedings of the 21st Annual Conference of ILASS Americas*, 2008.

[6] D. Kim, O. Desjardins, M. Herrmann, and P. Moin. The primary breakup of a round liquid jet by a coaxial flow of gas. *Proceedings of the 2oth Annual Conference of ILASS Americas*, 2007.

[7] P. Spiekermann, S. Jerzembeck, C. Felsch, S. Vogel, M. Gauding, and N. Peters. Experimental data and numerical simulation of common-rail ethanol sprays at diesel engine-like conditions. *Atomization and Sprays*, 19:357–387, 2009.

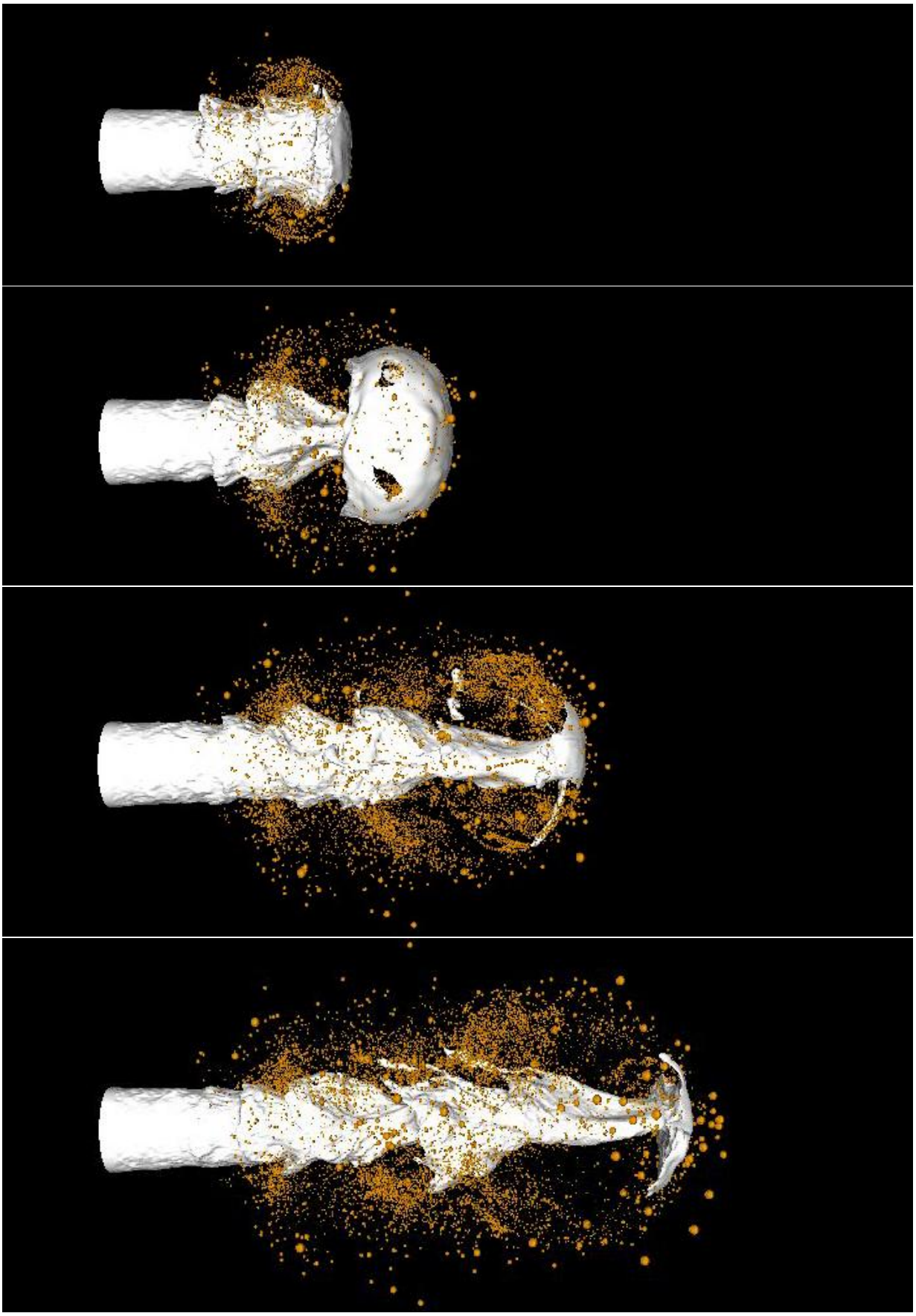

Figure 9: Four successive snapshots of primary atomization, from top to bottom, $t = 4\mu s$,$t = 6\mu s$,$t = 8\mu s$,$t = 10\mu s$